metals

MDPI

Article

The Effect of Forging and Heat Treatment Variables on Microstructure and Mechanical Properties of a Re-Bearing Powder-Metallurgy Nickel Base Superalloy

Shamil Mukhtarov [1,*], Dmitry Karyagin [2], Artem Ganeev [1], Rishat Zainullin [1], Ruslan Shakhov [1] and Valery Imayev [1]

[1] Institute for Metals Superplasticity Problems of Russian Academy of Sciences, Ufa 450001, Russia; artem@imsp.ru (A.G.); shakhov@imsp.ru (R.S.)
[2] CMK, Stupino 142800, Russia
* Correspondence: shamil@anrb.ru; Tel.: +7-347-282-38-19

Abstract: In our previous works, the effects of forging and heat treatment variables on microstructure evolution and mechanical properties have been studied for an ingot-metallurgy Re-bearing nickel base superalloy. To overcome the issues associated with the production of large-scale ingots and fine-grained workpieces, in the present work, the effect of hot forging and heat treatment variables was studied in a Re-bearing nickel base superalloy prepared via powder metallurgy. The purpose of the study was to reach the properly balanced mechanical properties for the potential use of the superalloy as a disc material. The initial as-HIPed workpieces were subjected to different hot forging and post-forging heat treatment or only to heat treatment (no forging). For the processed workpieces, the recrystallization behavior, size, morphology and volume fraction of γ' precipitates were evaluated by scanning electron microscopy followed by a study of mechanical properties. The most properly balanced mechanical properties (strength, ductility, creep resistance and creep rupture lifetime) were reached for the γ grain size of $d_\gamma \approx 13.6$ μm. A finer and coarser γ grain size (down to $d_\gamma \approx 2.6$ and up to $d_\gamma \approx 37.5$ μm) even when superimposed with a higher volume fraction of dispersed secondary γ' precipitates (in the case of d_γ = 27–37.5 μm) was associated with worse mechanical properties.

Keywords: nickel base superalloy; powder metallurgy; microstructure; forging; heat treatment; tensile properties; creep properties

Citation: Mukhtarov, S.; Karyagin, D.; Ganeev, A.; Zainullin, R.; Shakhov, R.; Imayev, V. The Effect of Forging and Heat Treatment Variables on Microstructure and Mechanical Properties of a Re-Bearing Powder-Metallurgy Nickel Base Superalloy. *Metals* **2023**, *13*, 1110. https://doi.org/10.3390/met13061110

Academic Editor: Zbigniew Pater

Received: 23 May 2023
Revised: 7 June 2023
Accepted: 10 June 2023
Published: 13 June 2023

1. Introduction

Creating a new generation of gas turbine engines (GTE) and similar energy-conversion systems with improved operating efficiency depends on the development of new materials with enhanced strength, heat resistance, and/or reduced specific weight. For instance, the operating efficiency of a GTE will increase by over 1% for every 10 °C increase in the turbine-inlet temperature [1]. In particular, ever-increasing demands are being placed on nickel base superalloys, which are widely used for the manufacturing of rotary engine parts such as high-pressure discs in GTE [2,3]. For this purpose, experimental heavily alloyed disc superalloys doped with Re have been recently designed [4–8]. Rhenium is known to be a quite unique alloying element regarding nickel base superalloys. It is known that it is typically found in the matrix γ phase, providing significant solid solution hardening and slowing down diffusion processes in the γ phase and at interphase boundaries, contributing to an increase in the strength and creep resistance of superalloy [9–11]. Rhenium is now added both to powder-metallurgy (PM) [6–8] and ingot-metallurgy (IM) [4,5] superalloys. In our previous works, the effect of forging and heat treatment variables on microstructure evolution and mechanical properties has been studied for an IM Re-bearing nickel base superalloy SDZhS-15 [4,5]. The superalloy showed excellent tensile properties in a fine-grained condition ($d_\gamma \approx$ 5–15 μm), whereas a larger γ grain size led to a rather significant

decrease in strength, ductility and creep rupture lifetime [4]. From a general point of view and considering our previous work [4], one may suppose that the alloying of nickel base superalloys with refractory elements such as tungsten, molybdenum and especially rhenium having a strong partitioning preference $\gamma > \gamma'$ can decrease the "optimal" size of γ grains, providing properly balanced mechanical properties. In the present work, this idea was tested for a Re-bearing PM nickel base superalloy close to the composition of the SDZhS-15 superalloy. The following considerations motivated the choice of the PM superalloy. The γ grain size in a PM superalloy is easier reached and controlled than in an IM superalloy considering the issues associated with the production of a fine-grained workpiece from an ingot having a coarse-grained structure and a strong dendritic segregation. In addition, the fabrication of ingots with a diameter $\geq$200 mm from heavily alloyed nickel base superalloys such as SDZhS-15 is also a great issue hindering the commercialization of such superalloys.

In the Re-bearing PM superalloy under study, the content of (Al + Ti + Nb + Ta) is 16.8 at. % and the ratio (Ti + Nb + Ta)/Al (in at. %) is 0.92, showing a strong solid solution hardening of the γ' phase. The γ matrix chemistry was optimized through a careful balance between the solid solution elements, such as Cr, Co, Mo, W, and Re. Generally, alloying was aimed to: (i) increase the volume fraction of the γ' phase, (ii) increase the solid solution hardening of both the γ matrix and the γ' phase, (iii) maintain oxidation and corrosion resistances via significant alloying with Cr, and (iv) avoid the formation of undesirable topologically close packed (TCP) phases. Thus, the present work aimed to study the effect of forging and heat treatment variables on the microstructure and mechanical properties of the PM Re-bearing nickel base superalloy. The heat treatment included different solid solution treatment followed by air cooling at a certain cooling rate and aging. Tensile and creep properties including the creep rupture lifetime of the superalloy were evaluated in different microstructural conditions. The study was finally aimed at reaching the most favorable microstructural conditions for properly balanced mechanical properties for the potential use of the superalloy as a disc material.

2. Materials and Methods

2.1. Initial Material

The nominal composition of the experimental PM nickel base superalloy was Ni-16(Al,Ti,Nb,Ta)-30(Cr,Co,Mo,Hf,W,Re) (wt. %). The exact composition of the superalloy is not indicated for confidential reasons. The initial powders had a spherical shape without any sticking and inclusions on the surface of the powders. The powders had a size ranging from 20 to 100 μm with 80% of the powders having a size of 40 to 71 μm. The bulk density of the powders without and after vibrocompaction was 4.97–5.04 g/cm^3 (≈60%) and about 5.6 g/cm^3 (≈67%), respectively. The initial powders were consolidated by hot isostatic pressing (HIP) at 1245 °C/170 MPa for 4 h. As a result, cylinders with a size of Ø100 mm × 200 mm were manufactured. The porosity of the as-HIPed material was no more than 0.3%. The alloy composition measured by energy dispersive X-Ray (EDS) analysis was very close to the nominal composition. The γ' solvus temperature (T_s) defined via quenching experiments from temperatures 1200 °C to 1250 °C was defined as $T_s \approx 1240 \pm 5$ °C [8].

2.2. Processing Methods

The as-HIPed material prior forging was homogenized at T = 1220 °C for 15 h, which was followed by slow cooling in the furnace. From the homogenized material, the billets with a size of Ø37 mm × 50 mm were cut and put into a can made of a stainless steel. The can was used to maintain the quasi-isothermal conditions and creating quasi-hydrostatic pressure during forging. Before forging, the die tool was heated up to 950 °C. The canned billets were subjected to three-stage unidirectional quasi-isothermal forging at subsolvus temperatures with intermediate recrystallization annealing, which was followed by decanning and heat treatment. In summary, three temperature conditions were used for forging: 1225–1200 °C, 1200–1175 °C and 1200–1150 °C, so the forging temperature

gradually decreased from stage to stage within one of the indicated temperature intervals. Thus, the final forging temperatures corresponding to three forging procedures (designated below as F1, F2 and F3) were 1200, 1175 and 1150 °C. Between forging stages, the canned workpieces were reheated in air. The total strain value and the average strain rate used in the forging procedures were always $e \approx 1.6$ and $\dot{\varepsilon} \approx 10^{-2}$ s^{-1}, respectively. As a result, sound forgings with a size of about Ø80 mm × 10 mm were obtained. Note that the forging procedure was earlier developed on the basis of compression tests of superalloy samples at subsolvus temperatures [8].

The post-forging heat treatment included a solid solution treatment at 1150–1260 °C ((T_s – 90)–(T_s + 20)), which was followed by cooling in air and aging or only aging. In order to preserve the refined structure, the solutioning heat treatment at subsolvus temperatures ((T_s − 90)–(T_s − 10)) was performed for 1 h and at solvus and supersolvus temperatures (T_s–(T_s + 20)) for a shorter tome, during 10–30 min. The forged workpieces had the same size, and the cooling rate in air applied after solution treatment was the same in the range of 2–5 °C/s during cooling from the solution treatment temperature to about 800 °C. The aging treatment was performed in two stages as is typically carried out for nickel base superalloys to completely precipitate the γ′ phase [12,13]. The first stage was conducted at 850 °C (10 h), and the second stage was conducted at 750 °C (50 h). To evaluate the effect of forging on the mechanical properties, the as-HIPed material was also subjected only to heat treatment, which included solid solution treatment at 1220 or 1230 °C ((T_s − 20)–(T_s − 10)) (2 h), which was followed by cooling in air and aging. In this case, the workpieces with a size of 60 mm × 60 mm × 10 mm were cut from the as-HIPed material that provided nearly the same cooling rate from the solution treatment temperature as in the case of the forged workpieces. All heat treatments were carried out in air.

The porosity in the forged and heat treated conditions remained near the same as in the as-HIPed condition and was no more than 0.3%.

2.3. Microstructural Examination

The microstructure was studied by scanning electron microscopy (SEM) in the back-scattering electron (BSE) and the secondary electron (SE) mode in a Tescan Mira-3 microscope (TESCAN, Brno-Kohoutovice, Czech Republic). SE and BSE images were used to evaluate the γ grain size, fraction, distribution and sizes of the coarse primary and dispersed secondary and tertiary γ′ phase. To estimate the mean size of γ grains, the sizes of the γ′ phase, and the volume fraction of each phase, the intercept method was applied. For this purpose, the samples subjected to mechanical polishing were used. BSE images at lower magnifications were mostly used to define the mean size of γ grains, and SE images at higher magnifications were used to determine the sizes of the primary and secondary (tertiary) γ′ phase and the volume fraction of each phase. The primary and secondary γ′ were distinguished reasoning from the following considerations assumed for nickel base superalloys. Relatively coarse particles of the γ′ phase, which typically remain undissolved during the solutioning stage, delineate the γ grain boundaries. This is referred to as primary γ′ precipitation. An intragranular γ′ phase forms on cooling and typically has a bimodal distribution including secondary γ′ and dispersed tertiary γ′ [14]. Not less than 300 γ grains were taken into account when estimating the mean size of γ grains (in the microstructural conditions not subjected to forging) or the mean size of recrystallized γ grains (in the conditions subjected to forging). To evaluate the development of recrystallization processes, the electron backscatter diffraction (EBSD) analysis was performed with a scan-step size of 0.5 μm using the HKL Channel 5 software (Oxford Instruments HKL, Hobro, Denmark). In addition to EBSD maps, the Kernel Average Misorientation (KAM) maps were drawn. In the inverse-pole-figure maps, the grain/interphase boundaries having a misorientation angle of less than 2° were excluded from the data analysis considering the experimental error in evaluating orientations by EBSD [15]. In the KAM maps, the misorientation angles less than 2° were taken into consideration. The grain/interphase boundaries having a misorientation angle of more than 15° were assumed as high-angle ones.

2.4. Mechanical Tests

The flat samples for tensile tests were cut from the processed workpieces. The specimens having gauge sections of 2 mm × 3 mm × 10 mm and 3 mm × 3 mm × 17 mm were used for tensile tests and creep tests, respectively. The total length of the specimens including grips was 35 and 45 mm for tensile and creep tests, respectively. Before testing, all surfaces of the specimens were mechanically polished down to a 4000 grit finish using SiC paper. The tensile tests were performed at T = 20, 650, and 750 °C using an Instron 5982 (Instron, Norwood, MA, USA). Not less than 3 samples per point were tensile tested. The creep tests were carried out at 750 °C/765 MPa. A total of 1–2 creep specimens per point were tested. The two-arm load machine having a lever arm ratio of 20:1 was used for the creep tests. All mechanical tests were carried out in the air.

The regression Larson–Miller equations of the superalloy are given from creep life ranging from 650 to 750 °C at different stresses (700–1178 MPa). A Larson–Miller parameter (LMP) relationship was calculated by the following equation [16–18]:

$$LMP = T \times [\log t_{rup} + 20], \quad (1)$$

where T is the creep testing temperature in K, and t_{rup} is the creep rupture life in hours.

3. Results and Discussion

3.1. Microstructure Characterization

3.1.1. As-Received HIPed and Homogenized Microstructural Conditions

Figure 1a,b show the superalloy microstructure in the initial as-HIPed condition. The as-HIPed condition had a mean γ grain size of $d_\gamma \approx 27$ μm. The γ grain boundaries were precipitated by the primary γ′ phase with a size of $d_{\gamma'}$ = 3–20 μm. The fraction of the primary γ′ phase was defined as about 11%. The presence of the high-volume fraction of coarse primary γ′ phase suggests that HIPing was followed by slow cooling. The secondary and tertiary γ′ phase precipitates with a size of 0.2–1.5 μm and smaller than 0.1 μm, respectively, were observed within γ grains. Some secondary γ′ precipitates had a dendritic form (Figure 1b). Carbide particles with a size of 1–8 μm were observed. The volume fractions of the γ′ phase and carbide particles were defined as about 75% and not more than 1%, respectively [8]. Unfavorable TCP phases were not detected.

Figure 1c,d represents the microstructural condition obtained after homogenization annealing, which was followed by slow cooling. Annealing led to the growth of γ grains up to $d_\gamma \approx 42$ μm, to slight coarsening of the primary γ′ phase along γ grain boundaries up to 5–20 μm and to an increase in the volume fraction of the primary γ′ phase up to about 26%. The secondary and tertiary γ′ phase particles with a size of 0.5–4 μm and smaller than 0.1 μm, respectively, were precipitated within γ grains (Figure 1d). Table 1 shows the microstructural parameters obtained in workpieces of the superalloy in the initial as-HIPed and homogenized conditions.

Table 1. Microstructural parameters obtained in workpieces of the superalloy after homogenization and forging with intermediate annealing (d_γ is the mean γ grain size or the mean size of recrystallized γ grains, $d_{\gamma'}$(I) is the size of the primary γ′ phase, $d_{\gamma'}$(II) is the size of the secondary/tertiary γ′ precipitates, $V_{\gamma'}$(I) is the volume fraction of the primary γ′ phase, and η is the fraction of high-angle grain/interphase boundaries (defined by EBSD analysis)).

Processing Route	Forging Temperature, °C	d_γ, μm	$d_{\gamma'}$(I), μm	$d_{\gamma'}$(II), μm	$V_{\gamma'}$(I), %	η, %
HIP [1]	-	27	3–20	0.2–1.5	11	-
HIP + HA [2]	-	42	5–20	0.5–4	26	-
HIP + HA + F1 [3]	1225–1200	4	1–20	0.1–0.3	20	66.5
HIP + HA + F2	1200–1175	3.8	1–20	0.1–0.3	35	68.9
HIP + HA + F3	1200–1150	2.6	1–20	0.1–0.3	46	70.4

[1] HIP—hot isostatic pressing, [2] HA—homogenization annealing, [3] F(1–3)—forging at different temperatures with intermediate annealing.

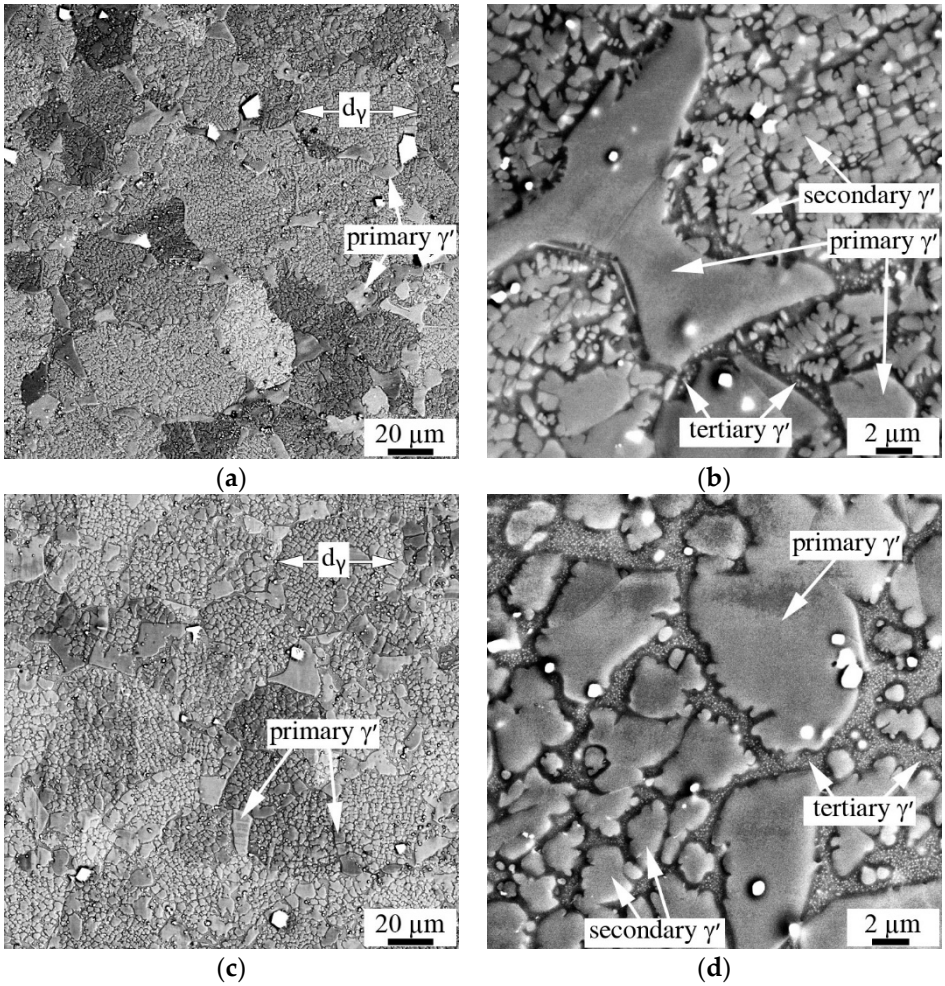

Figure 1. (**a**,**c**) BSE and (**b**,**d**) SE images of the superalloy: (**a**,**b**) the initial as-HIPed condition; (**c**,**d**) the HIPed and homogenized condition. Arrows show the typical γ grains and primary, secondary and tertiary γ′ phases.

3.1.2. Effect of Hot Forging on the Microstructure

Three forging procedures were applied to reach recrystallized, homogeneous and fine-grained structures with a different γ grain size. As mentioned, all forging procedures were carried out at subsolvus temperatures with intermediate recrystallization annealing as described elsewhere [8] and with decreasing the forging temperature from stage to stage. Microstructure examination showed that all forging processes led to the occurrence of dynamic recovery and recrystallization, resulting in the refinement of the initial microstructure. As was shown in our previous works [5,8,19], the use of fractional forging with intermediate recrystallization annealing and the massive can made of a stainless steel contributed to the formation of a homogeneous recrystallized microstructure throughout the forgings. However, coarse non-recrystallized γ grains with a size of 30–50 μm were also observed in the forgings. By way of illustration, Figures 2 and 3 show the typical EBSD- and corresponding KAM-maps as well as the BSE and SE images of the superalloy after forging at 1225–1200 °C and 1200–1150 °C. Table 1 describes schematically the forging regimes and microstructural conditions obtained after forging. The decrease in the forging temperature led to a finer size of recrystallized γ grains and to higher volume fractions of coarse non-recrystallized γ grains and the primary γ′ phase (Figures 2 and 3). Apparently, a higher volume fraction of the undissolved γ′ phase at lower forging temperatures contributed to the strain localization, leading to an increase in the volume fraction of non-recrystallized γ grains. It is interesting to note an increase in the volume fraction of the coarse primary γ′ phase as the forging temperature decreased. Particularly, the volume fraction of the pri-

mary γ′ phase increased from ≈20 to ≈46% when the forging temperature decreased from 1225–1200 to 1200–1150 °C (Table 1). Most likely, the grain/interphase boundaries served as diffusion paths and contributed to the development of coalescence of the primary γ′ phase during forging and intermediate annealing. The fraction of high-angle grain/interphase boundaries was similar and varied in the range of 66.5–70.4%. This also confirms the occurrence of recrystallization processes during forging with intermediate annealing.

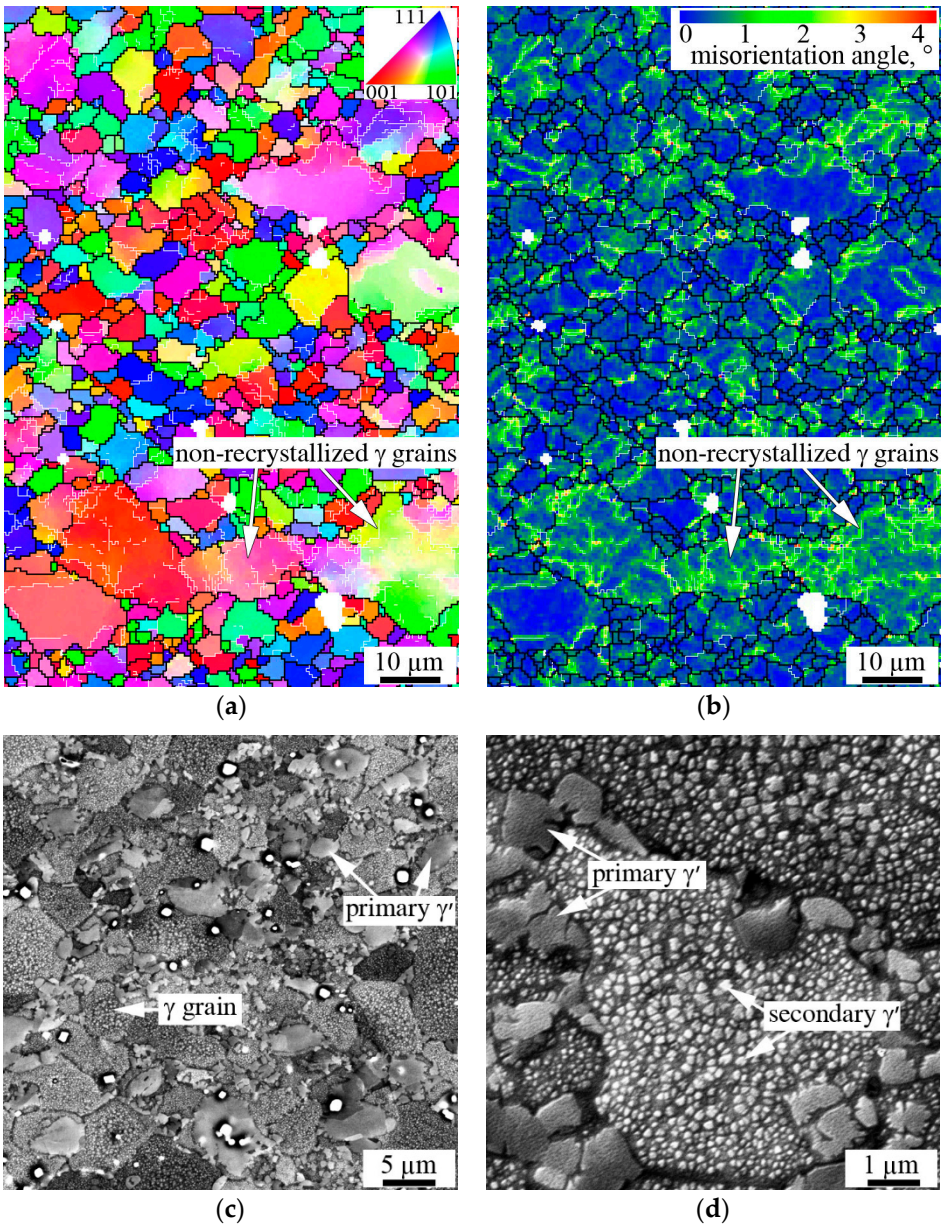

Figure 2. The microstructural images of the superalloy obtained from the central part of forging after homogenization annealing and forging at T = 1225–1200 °C ($\dot{\varepsilon} \approx 10^{-2}$ s^{-1}): (**a**) normal direction EBSD map (inverse pole figure) and (**b**) corresponding KAM map; (**c**) BSE; (**d**) SE. The forging axis is vertical. In (**a**), high- and low-angle grain/interphase boundaries are indicated by black and white lines, respectively. In (**b**), the green color shows the not completely recrystallized areas. Arrows show the elongated non-recrystallized and recrystallized γ grains, primary and secondary γ′ phase.

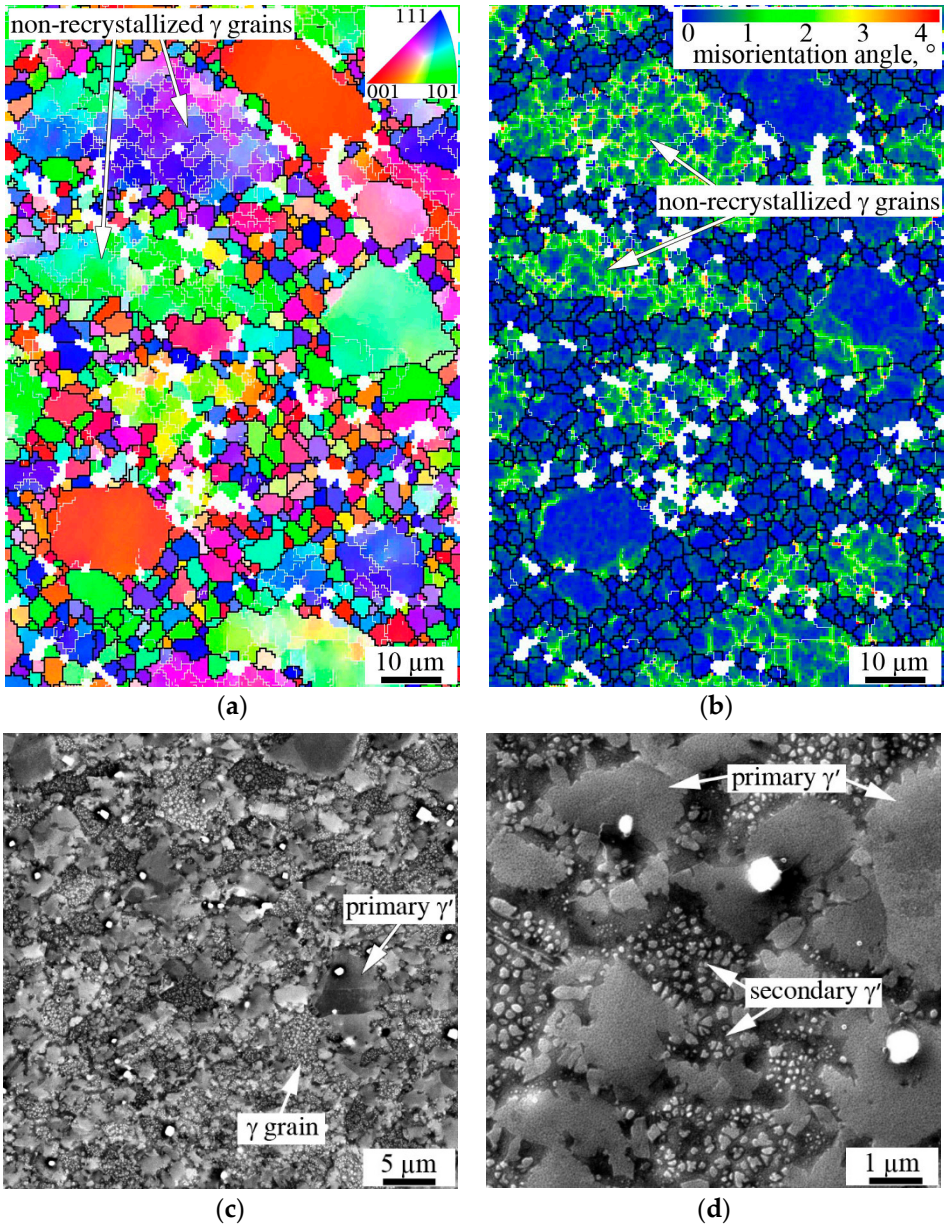

Figure 3. The microstructural images of the superalloy obtained from the central part of forging after homogenization annealing and forging at T = 1200–1150 °C ($\dot{\varepsilon} \approx 10^{-2}$ s^{-1}): (**a**) normal direction EBSD map (inverse pole figure) and (**b**) corresponding KAM map; (**c**) BSE; (**d**) SE. The forging axis is vertical. In (**a**), high- and low-angle grain/interphase boundaries are indicated by black and white lines, respectively. In (**b**), the green color shows not completely recrystallized areas. Arrows show the elongated non-recrystallized and recrystallized γ grains, primary and secondary γ′ phase.

3.1.3. Effect of Post-Forging Heat Treatment on the Microstructure

The forged workpieces were subjected to solution treatment followed by cooling in air and aging or only aging. In the last case, it was assumed that the solution heat treatment occurred after completing the forging and cooling of the forged workpiece in air. Table 2 describes schematically the processing and microstructural conditions obtained in the forged and heat treated workpieces. By way of illustration, Figures 4–7 show BSE and SE images of the superalloy after homogenization, forging and heat treatment (conditions 1 and 4–6).

Table 2. Processing and microstructural parameters obtained in workpieces of the superalloy after processing (d_{γ} is the mean γ grain size or the mean size of recrystallized γ grains, $d_{\gamma'}$(I) is the size of primary γ′ phase, $d_{\gamma'}$(II) is the size of secondary/tertiary γ′ precipitates, and $V_{\gamma'}$(I) is the volume fraction of the primary γ′ phase).

Condition Number	Processing Route	d_{γ}, μm	$d_{\gamma'}$(I), μm	$d_{\gamma'}$(II), μm	$V_{\gamma'}$(I), %
1	HIP [1] + ST [2] (1230 °C, 2 h), AC [3] + A [4]	33	1–20	0.2–0.3	7
2	HIP + ST (1220 °C, 2 h), AC + A	27	1–20	0.2–0.3	10
3	HIP + HA [5] + F1 [6] + ST (1230 °C, 1 h), AC + A	29.3	2–20	0.2–0.3	7
4	HIP + HA + F1 + ST (1210 °C, 1 h), AC + A	13.6	1–20	0.2–0.3	18
5	HIP + HA + F1 + A	4	1–20	0.05–0.3	20
6	HIP + HA + F2 + ST (1240 °C, 10 min), AC + A	37.5	1–4	0.1–0.25	5
7	HIP + HA + F3 + ST (1150 °C, 1 h), AC + A	5	1–20	0.15–0.3	40
8	HIP + HA + F3 + A	2.6	1–20	0.05–0.3	46

[1] HIP—hot isostatic pressing; [2] ST—solid solution treatment; [3] AC—air cooling; [4] A—aging; [5] HA—homogenization annealing; [6] F(1–3)—forging at different temperatures with intermediate annealing.

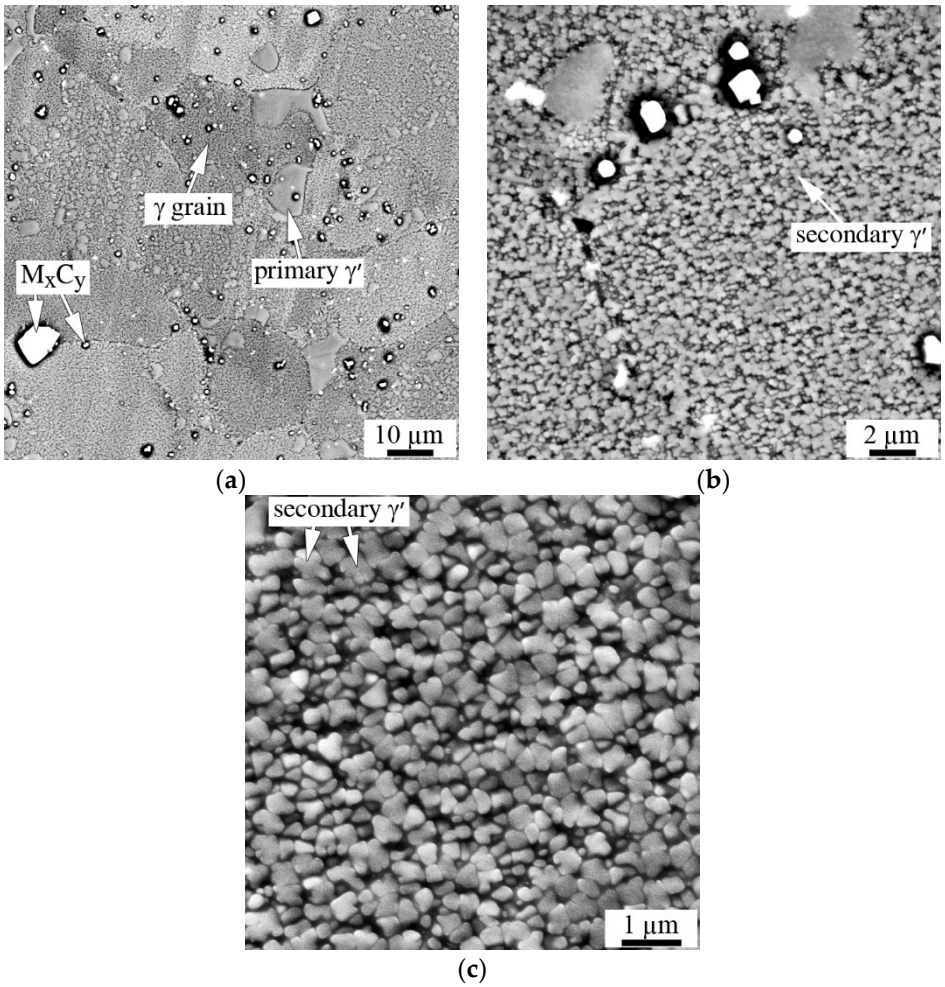

Figure 4. (**a**,**b**) BSE and (**c**) SE images of the superalloy in condition 1 obtained after HIPing, solution heat treatment at 1230 °C and aging. Arrows show the typical γ grain, primary and secondary γ′ phase and carbides.

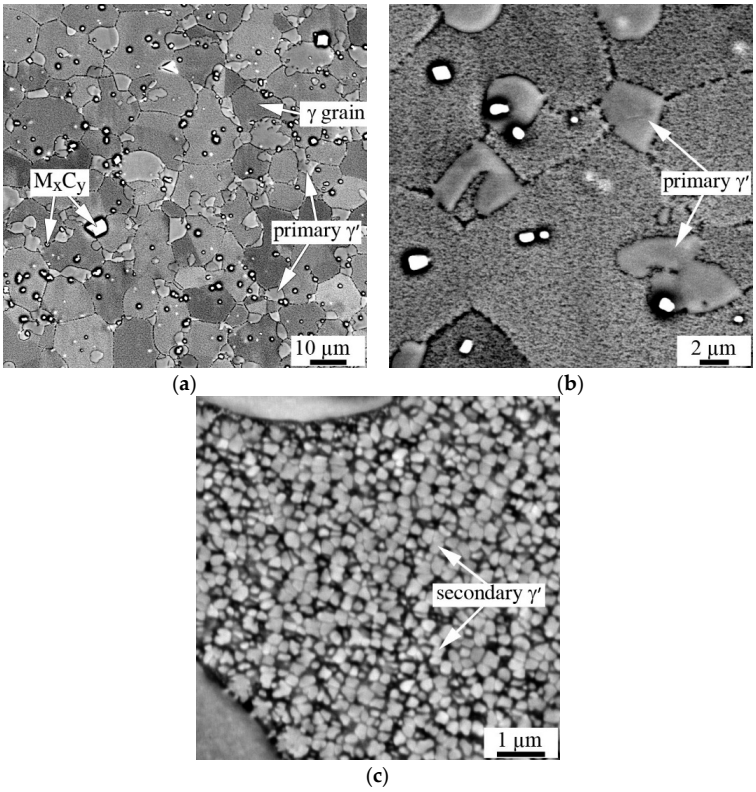

Figure 5. (**a**,**b**) BSE and (**c**) SE images of the superalloy in condition 4 obtained after forging (F1), solution heat treatment at 1210 °C and aging. Arrows show the typical γ grain, primary and secondary γ′ phase and carbides.

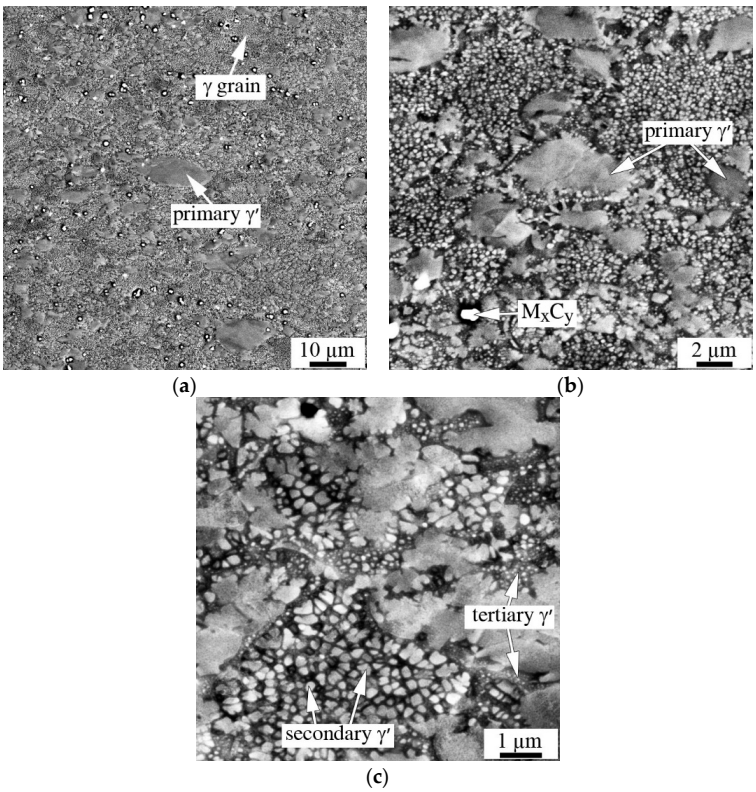

Figure 6. (**a**,**b**) BSE and (**c**) SE images of the superalloy in condition 5 obtained after forging (F1) and aging. Arrows show the typical γ grain, primary and secondary γ′ phase and carbides.

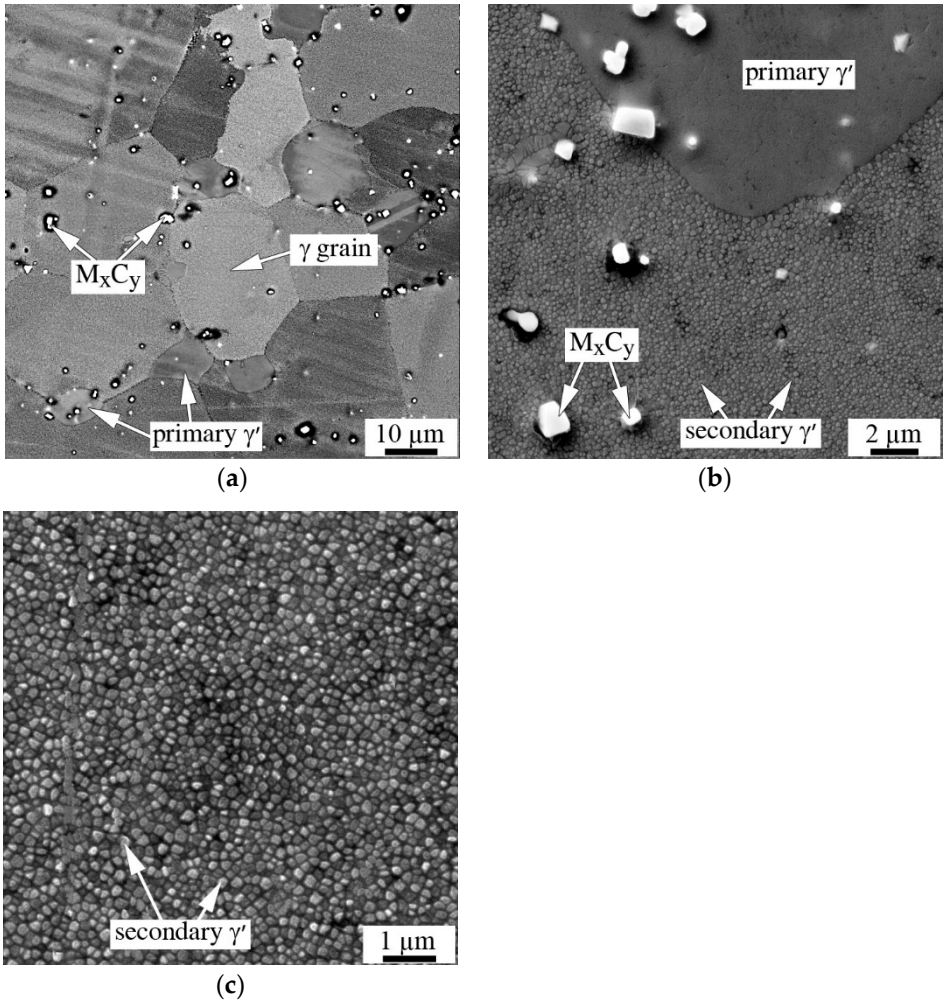

Figure 7. (**a**,**b**) BSE and (**c**) SE images of the superalloy in condition 6 obtained after forging (F2), solution heat treatment at 1240 °C and aging. Arrows show the typical γ grain, primary and secondary γ′ phase and carbides.

Figure 4 represents the BSE and SE images of condition 1 (Table 2). After solution treatment at 1230 °C and aging, the mean γ grain size was $d_\gamma \approx 33$ μm (Figure 4a), the size of the primary γ′ phase located along the γ grain boundaries was in the range of 1–20 μm (Figure 4b), and the size of the secondary γ′ precipitates was in the range of 0.2–0.3 μm (Figure 4c). The volume fraction of the coarse primary γ′ phase was about 7%. In the microstructure, there were coarse and fine carbide particles with sizes of 5–10 and 0.5–1 μm, respectively; their volume fraction was not more than 1%.

Figure 5 shows the BSE and SE images of condition 4 (Table 2). Solution treatment at a lower temperature (1210 °C) led to a higher amount of the undissolved primary γ′ phase and, therefore, the fine-grained microstructure obtained after forging was somewhat retained. The mean size of recrystallized γ grains was $d_\gamma \approx 13.6$ μm (Figure 5a), the size of the primary γ′ phase was in the range of 1–20 μm (Figure 5b), and the size of the secondary γ′ precipitates was in the range of 0.2–0.3 μm (Figure 5c). The volume fraction of the primary γ′ phase was about 18%. The size and the volume fraction of carbide particles were approximately the same as in condition 1.

Figure 6 represents the BSE and SE images of condition 5 (Table 2). Post-forging aging did not cause grain growth as solution heat treatment. The mean size of recrystallized γ grains remained $d_\gamma \approx 4$ μm, as was after forging (Figure 6a). The size of the primary γ′ phase was in the range of 1–20 μm (Figure 6b), and its volume fraction was about 20%. The size of the secondary and tertiary γ′ precipitates was in the range of 0.05–0.3 μm (Figure 6c).

The size and the volume fraction of carbide particles were approximately the same as in the previous conditions.

Figure 7 shows the BSE and SE images of condition 6 (Table 2). Post-forging short-time solution treatment at γ' solvus temperature (T = 1240 °C) led to the partial dissolution of the γ' phase, and the mean size of recrystallized γ grains increased up to d ≈ 37.5 μm (Figure 7a). The fact that the γ' phase was not completely dissolved can be ascribed to a short time (10 min) of the solution treatment at 1240 °C. The size of the primary γ' phase decreased down to 1–4 μm (Figure 7b), and its volume fraction was about 5%. The size of the secondary γ' precipitates was in the range of 0.1–0.25 μm (Figure 7c). The size and the volume fraction of carbide particles were approximately the same as in conditions 1, 4 and 5. Coarse non-recrystallized γ grains were preserved in conditions 4, 5, 7 and 8. TCP phases were not detected in all conditions. The solution heat treatment of the HIPed condition at supersolvus temperatures (1250–1260 °C, 30 min) led to the complete dissolution of the γ' phase and the γ grain growth up to around 50 μm and was not considered for mechanical properties.

Analysis of the obtained microstructural conditions and comparison with the as-forged conditions (Table 1) allows us to draw the following conclusions:

- Solution treatment led to the development of recrystallization processes and γ grain growth. As the solution treatment temperature increased, the grain growth occurred faster. With increasing the solution treatment temperature from 1150 to 1240 °C, the mean size of recrystallized γ grains increased from 5 to 37.5 μm. Note that solution treatment at 1240 °C would cause a larger γ grain size if the longer solution treatment was applied;
- Solution treatment at 1220–1240 °C (($T_s - 20$)–($T_s - 10$)) followed by aging (conditions 1–3 and 6) resulted in nearly the same size and morphology of the primary γ' phase and nearly the same size and irregular round morphology of the secondary γ' precipitates;
- Forging at 1225–1200 °C followed by solution treatment at 1210 °C ($T_s - 30$) and aging or only aging (conditions 4 and 5) gave nearly the same characteristics of the primary and secondary γ' phase. Particularly, the volume fraction of the primary γ' phase was 18–20%;
- Forging at 1200–1150 °C followed by solution treatment at 1150 °C and aging or only aging (conditions 7 and 8) also gave near the same characteristics of the primary and secondary γ' phase. Particularly, the volume fraction of the primary γ' phase was defined as 40–46%. Some difference between the conditions subjected to solution treatment and aging in contrast to the conditions subjected only to aging consisted of the appearance of dispersed tertiary precipitates of the γ' phase in the last case. Taking into consideration the size and morphology of the γ' phase, all conditions can be divided into three groups: conditions 1–3 and 6 (group 1), conditions 4 and 5 (group 2), and conditions 7 and 8 (group 3). Thus, the volume fraction of the primary γ' phase depended on the solution treatment temperature;
- Aging immediately after forging did not have an influence on the γ grain size and the volume fraction of the primary γ' phase. The fact is that aging was conducted at relatively low temperatures and almost did not lead to dissolution of the γ' phase. Therefore, the γ grain size was not changed after aging (conditions 5 and 8) as compared to the forged conditions;
- The size and the volume fraction of carbide particles were approximately the same in all microstructural conditions;
- Unfavorable TCP phases were not detected in all microstructural conditions.

Thus, considering the size and the volume fraction of the γ' phase, the most favorable microstructures were reached in conditions 1–3 and 6, in which the volume fraction of the coarse primary γ' phase was in the range of 5–10%. Fine-grained conditions 4, 5, 7 and 8 (d_γ = 2.6–13.6 μm) contained 18–46 vol.% of the primary γ' phase that is not to be favorable for creep properties.

Figure 8 represents the dependences of the mean size of recrystallized γ grains or the mean γ grain size on the last forging temperature and/or the solution treatment

temperature. As mentioned, aging did not have any influence on the γ grain size. With increasing the last forging temperature and/or the solution treatment temperature, the γ grain size increased, reaching $d_\gamma \approx 50$ μm after solution treatment at 1260 °C (30 min). The solution treatment temperature was the major factor determining the γ grain size for the forged conditions. The microstructure remained fine-grained if the solution treatment was carried out at T ≤ 1210 °C and became coarse-grained if the solution treatment was performed at T = 1230–1250 °C. Note that the γ grain growth after solution heat treatment in the PM Re-bearing superalloy under study was much less significant than in the IM Re-bearing superalloy studied in our previous work [4]. The solution treatment temperature influenced the γ grain size after HIPing without forging as well. The mean γ grain size increased from $d_\gamma \approx 27$ to ≈ 50 μm when the solution treatment increased from 1220 ($T_s - 20$) to 1260 °C ($T_s + 20$). The forging temperature in the range of 1150–1200 °C had a weak influence on the γ grain size. Note that the dependence of the γ grain size on the last forging or solution treatment temperature in the temperature range of 1150–1210 °C is somewhat conditional because non-recrystallized γ grains were retained, and the volume fraction of the primary γ′ phase was different in the fine-grained conditions. Nevertheless, taking into account that the size and the volume fraction of the primary γ′ phase was similar in conditions 1–3 and 6 (group 1), in conditions 4 and 5 (group 2), and in conditions 7 and 8 (group 3), we can consider the mechanical properties of the superalloy as a function of the γ grain size (keeping in mind different volume fractions of the primary γ′ phase in groups 1–3 and remaining individual non-recrystallized grains in the fine-grained conditions).

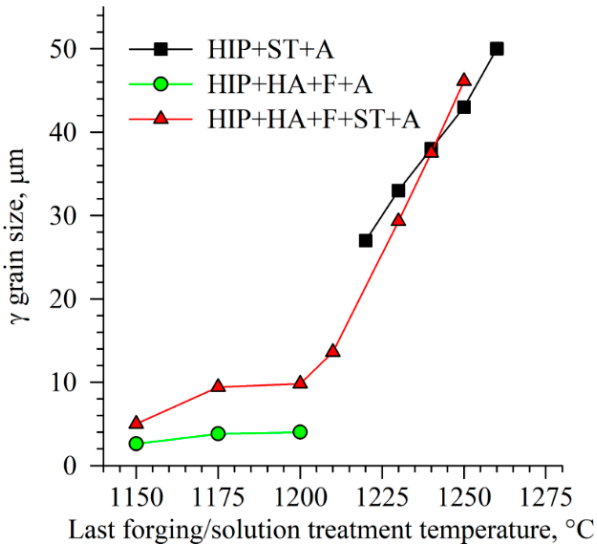

Figure 8. Dependences of the mean size of recrystallized γ grains or the mean γ grain size on the last forging temperature and/or the solution treatment temperature obtained for the superalloy after different processing (HIP—hot isostatic pressing; ST—solid solution treatment; A—aging; HA—homogenization annealing; F—forging at different temperatures with intermediate annealing).

3.2. Mechanical Properties

3.2.1. Tensile Properties

Figure 9 represents the averaged results of tensile tests shown as the dependences of the ultimate tensile strength (UTS), yield strength (YS) and elongation (A) on the γ grain size. With increasing the test temperature, the elongation and the UTS values decreased and the yield strength increased for the conditions with d_γ = 2.6–27 μm reaching the highest values at 650 °C and decreased for the conditions with d_γ = 33–37.5 μm. The observed tensile properties are quite typical of nickel base superalloys [20,21]. Particularly, the yield strength anomaly can be explained by a high volume fraction of the intermetallic γ′ phase, the yield strength of which increased with increasing the test temperature due to the thermally activated cross-slip of superdislocations leading to hindering the dislocation motion [22]. Apparently,

the cross-slip of superdislocations occurred less extensively in the coarse-grained conditions with a higher volume fraction of secondary γ′ precipitates that obscured the effect of the yield strength anomaly. Although the properties weakly depended on the γ grain size, one can see that slightly higher tensile properties (UTS, YS and A) at room temperature were reached in the fine-grained conditions with the γ grain size of d_γ = 2.6–13.6 μm. Near the same or slightly higher strength properties at 650 and 750 °C were obtained in the fine-grained conditions, particularly in conditions 5 ($d_\gamma \approx 4$ μm) and 8 ($d_\gamma \approx 2.6$ μm). The positive effect of the fine-grained structure on ductility was revealed at elevated temperatures. For instance, the elongation obtained at 750 °C for conditions 1–4 and 6 (d_γ = 13.6–37.5 μm) was 0.8–2.2% against 3.6–5.5% for conditions 5, 7 and 8 (d_γ = 2.6–5 μm). One may suppose that grain/interphase boundary relaxation occurred in the fine-grained conditions at 750 °C that contributed to a more uniform occurrence of plastic deformation and higher elongations.

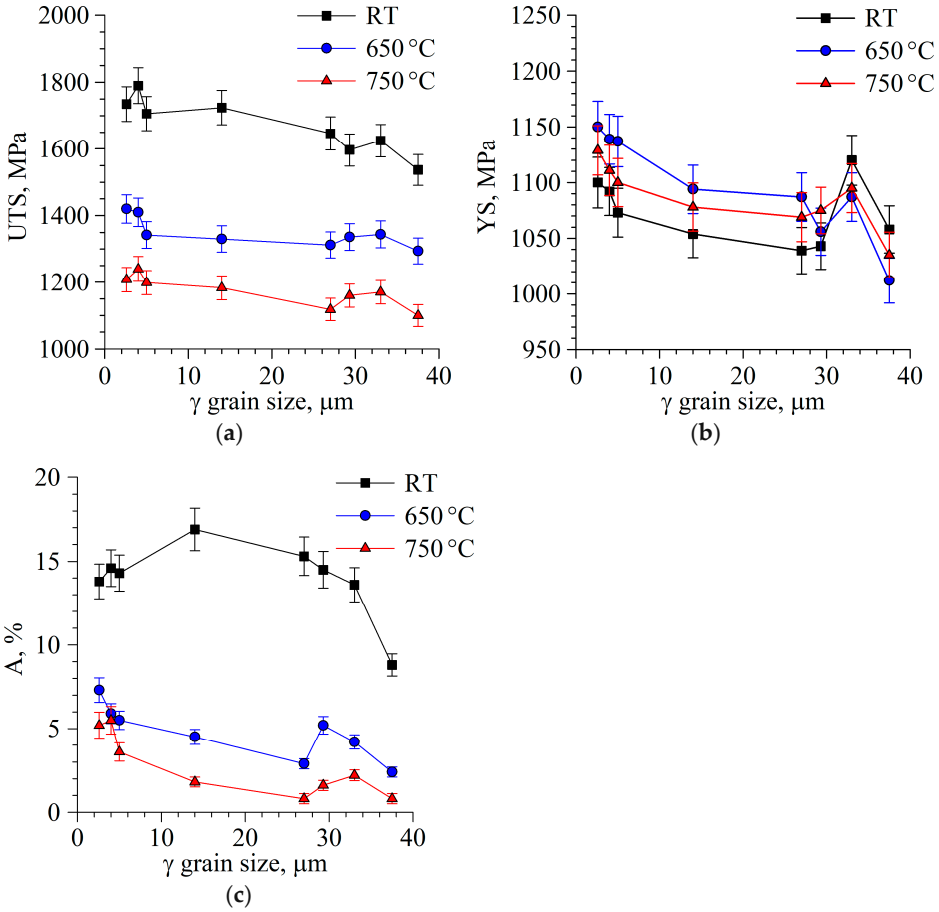

Figure 9. The averaged results of tensile tests as the dependences on the γ grain size: (**a**) UTS—ultimate tensile strength; (**b**) YS—yield strength; (**c**) A—elongation to rupture.

In general, the tensile properties depended not only on the γ grain size but also on the volume fraction of the primary γ′ phase. In contrast to the fine-grained conditions (4, 5, 7 and 8), the coarse-grained conditions (1–3 and 6) contained mostly a dispersed γ′ phase that provided more effective precipitation hardening than in the fine-grained conditions. Nevertheless, comparing the HIPed and heat treated conditions with the forged and heat treated conditions, the following considerations can be made regarding the dependence of the mechanical properties on the γ grain size:

- The strength properties (UTS, YS) were appreciably (by 6–12% for UTS) or slightly (YS) higher in the fine-grained conditions (d_γ = 2.6–13.6 μm) vs. coarse-grained ones (d_γ = 29–37.5 μm);

- The tensile properties were similar if the γ grain size was near the same (conditions 1–3): that is, the forging procedure did not improve the quality of the HIPed material when this did not result in a refined structure;
- The ductility in the fine-grained conditions (d_γ = 2.6–13.6 μm) in contrast to the coarse-grained conditions (d_γ = 27–37.5 μm) was slightly higher at room temperature (much higher than in condition 6, d_γ = 37.5 μm) and 650 °C, and it was appreciably higher at 750 °C;
- Irrespective of the γ grain size, the ductility decreased with increasing the test temperature from 20 to 750 °C (Figure 9c). The reason for the decrease in ductility is not completely clear. Note that a similar effect was also observed in some other superalloys, particularly in Inconel 718 [23,24].

3.2.2. Creep Properties

Figure 10 shows the creep curves obtained for conditions 1–5, 7 and 8 at 750 °C/765 MPa. Condition 6, which showed the lowest tensile properties, was not tested. The creep rate significantly decreased at the transition from fine-grained (d_γ = 2.6–5 μm) to coarse-grained conditions (d_γ = 27–33 μm). Condition 4 ($d_\gamma \approx$ 13.6 μm) showed the creep rate, which was very close to those obtained for coarse-grained conditions. Considering the creep properties, the following observations can be made:

- The creep curves were typical of polycrystalline nickel base superalloys;
- The creep load at 750 °C was high and the creep rate was rather high ($\dot{\varepsilon}_{creep} \sim 10^{-7}$ s^{-1}); therefore, creep rupture life was low (4.4–54.7 h) for all microstructural conditions;
- The creep curves obtained for the fine-grained conditions (d_γ = 2.6–5 μm) demonstrated short first and secondary stages, which were followed by an increase in the creep rate corresponding to the third stage. The finer the γ grain size, the shorter the first and secondary stages. This is associated with an extensive relaxation of stresses in the grain/interphase boundaries;
- For the creep curves obtained for the coarse-grained conditions (d_γ = 27–33 μm) the third stage of creep was not observed or was very short and these conditions showed the lowest creep rupture life (<15 h);
- The highest creep rupture life was reached for condition 4 ($d_\gamma \approx$ 13.6 μm) despite having a slightly higher creep rate in comparison with the coarse-grained conditions (d_γ = 27–33 μm). In this case, the secondary creep stage was the longest among the studied conditions;
- Coarse-grained conditions 1–3 ($d_\gamma \approx$ 27–33 μm) showed rather low creep rupture life in the interval of 4.4–14.5 h and a very close creep rate. As with the tensile properties, the creep resistance was similar if the γ grain size was near the same.

Thus, the best creep properties at 750 °C/765 MPa were achieved in condition 4 ($d_\gamma \approx$ 13.6 μm): the minimum creep rate and the creep rupture life were 1.7×10^{-7} s^{-1} and 54.7 h, respectively. A coarser γ grain size (d_γ = 27–33 μm) even superimposed with a higher volume fraction of dispersed secondary γ′ precipitates resulted in shorter creep rupture life. A finer γ grain size (d_γ = 2.6–5 μm) led to an increase in the minimum creep rate and a decrease in the secondary stage of creep that restricted the creep rupture life.

Taking into consideration the tensile properties, one can assume that the best combination of mechanical properties (strength, ductility, creep resistance and creep rupture life) showed condition 4 obtained via hot forging at 1225–1200 °C with intermediate annealing followed by solution treatment at 1210 °C and aging. This should be attributed to the relatively fine-grained structure ($d_\gamma \approx$ 13.6 μm), the high volume fraction of the secondary γ′ precipitates, and the relatively small volume fraction of the primary γ′ phase. Thus, the condition with the relatively fine-grained structure ($d_\gamma \approx$ 13.6 μm) containing about 18 vol.% of the primary γ′ phase showed the better creep rupture life and near the same minimum creep rate as the coarse-grained conditions with d_γ = 27–33 μm and the volume fraction of the primary γ′ phase of 5–10%. Apparently, as mentioned in the introduction, alloying with refractory elements, such as tungsten, molybdenum and especially rhenium

having a strong partitioning preference $\gamma > \gamma'$ (in [4], the averaged partitioning coefficient $k_{\gamma/\gamma'}$ obtained for rhenium was defined as 7.92) slowed down diffusion processes in the γ grains and at interphase boundaries that decreased the "optimal" size of γ grains down to $d_\gamma \approx 13.6$ μm, providing high creep resistance and creep rupture life. Comparing the condition with $d_\gamma \approx 13.6$ μm and the conditions with d_γ = 27–33 μm, one can conclude that the positive effect of the refined microstructure was more significant than the positive effect of a higher volume fraction of the secondary γ' precipitates obtained in the coarse-grained conditions.

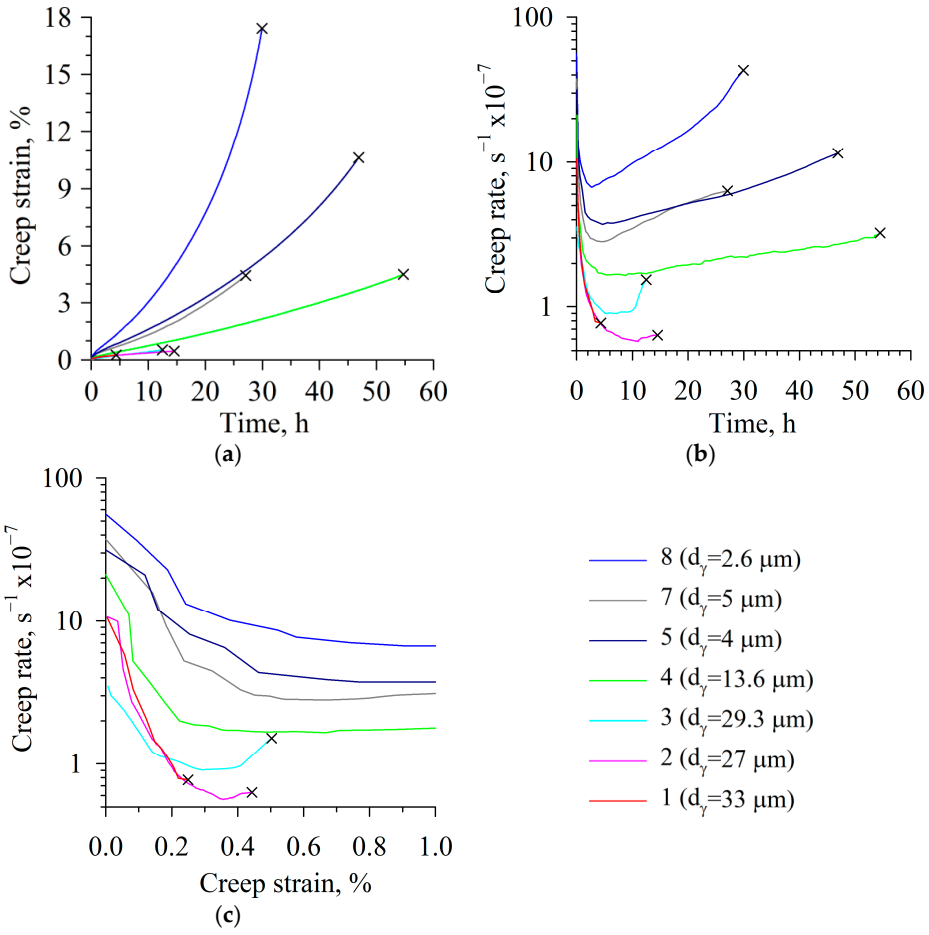

Figure 10. Creep behavior of the superalloy in conditions 1–5, 7, and 8 at 750 °C/765 MPa: (**a**) the creep strain vs. time; (**b**) the creep rate vs. time; (**c**) the creep rate vs. creep strain up to 1.0%. The points marked by a cross show the rupture of the specimens.

The obtained creep data were used to generate the dependencies of stress versus LMP, as calculated by Equation (1). The resulting plots are shown in Figure 11, and simple regression equations are included for estimating creep response at intermediate reply. Figures 10 and 11 indicate that the superalloy in the fine-grained conditions (d_γ = 2.6–5 μm) had a higher creep rupture life than that in the coarse-grained conditions (d_γ = 27–33 μm). However, the creep rate for the fine-grained conditions was appreciably higher than that for the coarse-grained conditions. Condition 4 ($d_\gamma \approx 13.6$ μm) showed the best combination of the creep rate and the creep rupture life. Taking into account the tensile properties, the optimal microstructural condition among the conditions under study should be assumed to be condition 4 obtained by forging at 1225–1200 °C followed by solution treatment at 1210 °C and aging. Note that similar values of LMP were also obtained for the disc superalloys N18 [25] and FGH 100 [26] (Figure 11).

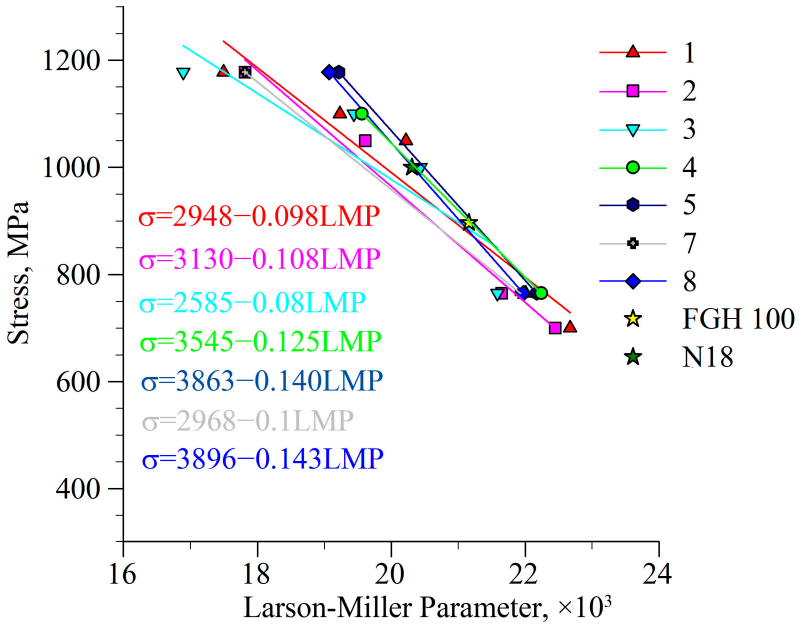

Figure 11. Larson–Miller parameter plotted for the superalloy under study in conditions 1–5, 7 and 8 and the other superalloys [25,26].

Thus, the presented results suggest that the "optimal" γ grain size for disc superalloys heavily alloyed with refractory elements and particularly with rhenium is $d_\gamma \approx 13.6$ μm, which is smaller than is typically considered for disc nickel base superalloys. Note that the gradient (or dual grain) structure is usually supposed in the turbine discs to have higher strength in the bore zone and higher creep resistance in the rim zone. Table 3 shows the γ grain sizes supposed for the bore and rim zones of turbine discs in different nickel base superalloys. It can be seen that most researchers consider d_γ = 4–20 μm for the bore zone and d_γ = 20–150 μm for the rim zone. The obtained results suggest that the "optimal" γ grain sizes for the bore and rim zones of a disc made of the PM superalloy under study are smaller than the typically considered γ grain sizes (Table 3). As mentioned, this is probably associated with high alloying of the superalloy with refractory elements and particularly with rhenium, which slowed down diffusion processes in the γ phase and at interphase boundaries, contributing to an increase in the creep resistance. Therefore, the "optimal" γ grain size providing the most properly balanced mechanical properties shifted toward smaller sizes.

Table 3. The γ grain sizes considered or recommended in different works with regard to the bore and rim zones of a turbine disc made of nickel base superalloys.

Superalloy	γ Grain Size in the Bore Zone, μm	γ Grain Size in the Rim Zone, μm	Refs.
Alloy 10 (PM)	5.6	31.8–44.9	[27]
RR 1000 (PM)	5–10	20–47	[28,29]
FGH 4096 (PM)	4	40	[30]
LSHR (PM)	4–8.4 (4–16)	31.8–63.5 (10–140)	[31,32]
GH4175 (IM)	20	113	[33]
PM superalloy of 3-rd generation	≤13	20–150	[34]
ME3 (Rene 104) (PM)	5	27.5	[35]
Russian superalloy EP741NP (PM)	5–13	45–70	[19]
Russian superalloy (PM)	2–5	10–15	This study

The volume fraction of the primary γ′ phase can be minimized by solution treatment at subsolvus temperatures slightly below the γ′ solvus temperatures or at supersolvus

temperatures. However, in the last case, a strong γ grain growth occurred, leading to a decrease in the tensile properties (strength and ductility) and did not provide higher creep rupture life. The microstructural condition with $d_\gamma \approx 13.6$ μm and containing a relatively high volume fraction of the primary γ' phase (about 18%) showed the best balanced mechanical properties.

4. Conclusions

The new experimental PM Re-bearing nickel base superalloy has been studied in the present work. The as-HIPed material was subjected to different forging procedures and heat treatments. As a result, a number of microstructural conditions with the γ grain size of d_γ = 2.6–37.5 μm and the fraction of the primary γ' phase ranging from 5 to 46% were obtained. The obtained microstructural conditions were characterized by SEM, and the tensile and creep tests were performed. The following conclusions can be drawn:

- The dependencies of the mechanical properties on the γ grain size were revealed despite the different volume fraction of the primary γ' phase in the obtained microstructural conditions. The fine-grained condition ($d_\gamma \approx 13.6$ μm) of the superalloy showed the most properly balanced mechanical properties. This microstructural condition was obtained using the following processing route: HIP + homogenization + forging in the temperature range of 1225–1200 °C + solution treatment at 1210 °C (1 h) followed by cooling in air + aging. For instance, the room temperature strength/ductility properties were UTS = 1720 MPa, YS = 1070 MPa, A = 17%. The creep rupture life at 750 °C/765 MPa was the highest among the studied conditions (54.7 h). The shift of the "optimal" γ grain size to smaller values than is typically considered for nickel base superalloys can be explained by higher alloying with refractory metals and, in particular, with rhenium.
- The forging procedure followed by heat treatment led to enhancement in the mechanical properties if the refined structure was produced. The coarse-grained microstructural conditions having near the same γ grain size and the similar distribution and volume fraction of the primary γ' phase showed very similar mechanical properties.
- The creep rate obtained for the coarse-grained conditions (d_γ = 27–33 μm) was near the same as for the condition with $d_\gamma \approx 13.6$ μm but appreciably lower than those obtained for the fine-grained conditions (d_γ = 2.6–5 μm). Nevertheless, the creep rupture life in the fine-grained conditions was found to be higher than in the coarse-grained conditions. The creep curves obtained for the coarse-grained conditions showed a very short secondary and third stage of creep or without the third stage that led to the lowest creep rupture life among the studied conditions (<15 h).
- The γ grain size is an important microstructural parameter determining the mechanical properties stronger than the fraction of the primary γ' phase. The microstructural condition with $d_\gamma \approx 13.6$ μm and containing a rather high volume fraction of the primary γ' phase (about 18%) showed the best balance of the mechanical properties.
- Based on the performed work, the recommended "optimal" γ grain sizes in the bore and rim zones of a turbine disc made of the PM superalloy under study are d_γ = 2–5 μm and d_γ = 10–15 μm, respectively. A refined structure can be obtained by canned forging in the temperature range of 1150–1225 °C followed by solid solution treatment at a temperature not higher than 1210 °C ($T_s - 30$) and aging or only aging. A refined structure can guarantee higher mechanical properties and reliability of the disc made of the PM superalloy.

Author Contributions: Conceptualization, S.M., V.I. and D.K.; methodology, A.G., R.S., R.Z., V.I. and S.M.; validation, A.G., D.K., V.I. and S.M.; formal analysis, V.I.; investigation, R.Z., R.S., A.G. and S.M.; writing—original draft preparation, S.M.; writing—review and editing, V.I. and S.M.; visualization, A.G. and R.S.; supervision, D.K.; project administration, V.I.; funding acquisition, S.M. All authors have read and agreed to the published version of the manuscript.

Funding: The work was supported by the Ministry of Science and Higher Education of the Russian Federation according to the State Assignment of the IMSP RAS (No. 122011900470-7).

Acknowledgments: The work was performed using the facilities of the shared services center "Structural and Physical-Mechanical Studies of Materials" at the Institute for Metals Superplasticity Problems of Russian Academy of Sciences.

Conflicts of Interest: The authors declare no conflict of interest.

References

1. Appel, F.; Paul, J.D.H.; Oehring, M. *Gamma Titanium Aluminide Alloys: Science and Technology*; Wiley-VCH Verlag GmbH & Co. KGaA: Weinheim, Germany, 2011; p. XIII. [CrossRef]
2. Reed, R. *The Superalloys: Fundamentals and Applications*, 1st ed.; Cambridge University Press: Cambridge, MA, USA, 2006; pp. 2–5. [CrossRef]
3. Pollock, T.M.; Tin, S. Nickel-based superalloys for advanced turbine engines: Chemistry, microstructure, and properties. *J. Propul. Power.* **2006**, *22*, 361–374. [CrossRef]
4. Imayev, V.; Mukhtarov, S.; Mukhtarova, K.; Ganeev, A.; Shakhov, R.; Parkhimovich, N.; Logunov, A. Influence of Forging and Heat Treatment on the Microstructure and Mechanical Properties of a Heavily Alloyed Ingot-Metallurgy Nickel-Based Superalloy. *Metals* **2020**, *10*, 1606. [CrossRef]
5. Mukhtarov, S.K.; Imayev, V.M.; Logunov, A.V.; Shmotin, Y.N.; Mikhailov, A.M.; Gaisin, R.A.; Shakhov, R.V.; Ganeev, A.A.; Imayev, R.M. Recrystallization behavior and mechanical properties of a novel Re-containing nickel base superalloy. *Mater. Sci. Technol.* **2019**, *36*, 1605–1613. [CrossRef]
6. Mourer, D.P.; Huron, E.S.; Backman, D.G.; Bain, K.R.; Reynolds, P.L.; Schirra, J.J.; Gabb, T.P. Ni Based Superalloy and Its Use as Gas Turbine Disks, Shafts, and Impellers. Patent EP No. 1195446 A1, 4 October 2000.
7. Mourer, D.P.; Huron, E.S.; Bain, K.R.; Montero, E.E.; Reynolds, P.L.; Schirra, J.J. Superalloy Optimized for High-Temperature Performance in High-Pressure Turbine Disks. Patent US No. 6,521,175 B1, 18 February 2003.
8. Mukhtarov, S.K.; Karyagin, D.A.; Logunov, A.V.; Ganeev, A.A.; Zainullin, R.I.; Shakhov, R.V.; Imayev, V.M. Effect of hot working on the microstructure and tensile properties of a novel PM Re-bearing nickel base superalloy. *Lett. Mater.* **2022**, *12*, 457–462. [CrossRef]
9. Mottura, A.; Reed, R.C. What is the role of rhenium in single crystal superalloys? *MATEC Web Conf.* **2014**, *14*, 01001. [CrossRef]
10. Wang, Y.-J.; Wang, C.-Y. The alloying mechanisms of Re, Ru in the quaternary Ni-based superalloys γ/γ' interface: A first principles calculation. *Mater. Sci. Eng. A* **2008**, *490*, 242–249. [CrossRef]
11. MacKay, R.; Gabb, T.; Garg, A.; Rogers, R.; Nathal, M. Influence of composition on microstructural parameters of single crystal nickel-base superalloys. *Mater. Charact.* **2012**, *70*, 83–100. [CrossRef]
12. Liu, F.; Wang, Z.; Tan, L.; Xiao, X.; Li, Y.; Li, X.; Zhang, H.; Zhu, L.; Jiang, L.; Liu, Y. Creep behaviors of fine-grained Ni-base powder metallurgy superalloys at elevated temperatures. *J. Alloys Compd.* **2021**, *867*, 158865. [CrossRef]
13. Bai, J.M.; Xing, P.Y.; Zhang, H.P.; Li, X.K.; Liu, J.T.; Jia, J.; Sun, Q.S.; Liu, C.S.; Zhang, Y.W. Effect of tantalum on the microstructure stability of PM Ni-base superalloys. *Mater. Charact.* **2021**, *179*, 111326. [CrossRef]
14. Jackson, M.P.; Reed, R.C. Heat treatment of UDIMET 720Li: The effect of microstructure on properties. *Mater. Sci. Eng. A* **1999**, *259*, 85–97. [CrossRef]
15. Humphreys, F.J. Quantitative metallography by electron backscattered diffraction. *J. Microsc.* **1999**, *195*, 170–185. [CrossRef] [PubMed]
16. Larson, F.R.; Miller, J. Time-temperature relationship for rupture and creep stresses. *Trans. ASME* **1952**, *74*, 765–775. [CrossRef]
17. Mataveli, L.S.; Cormier, J.; Villechaise, P.; Bertheau, D.; Benoit, G.; Cailletaud, G.; Marcin, L. Anisotropy in creep properties of DS200 + Hf alloy. *Mater. High Temp.* **2016**, *33*, 361–371. [CrossRef]
18. Radavich, J.; Furrer, D. Assessment of Russian P/M superalloy EP741NP. *Superalloys* **2004**, *2004*, 381–390. [CrossRef]
19. Ganeev, A.A.; Valitov, V.A.; Utyashev, F.Z.; Imayev, V.M. Effect of thermomechanical treatment on the formation of gradient structure and mechanical properties in a disk made of powder-metallurgy nickel-based superalloy. *Phys. Met. Met.* **2019**, *120*, 410–416. [CrossRef]
20. Mukhtarov, S.K. Effect of Grain Size on the Superplastic Behavior of a Nanostructured Nickel-Based Superalloy. *Mater. Sci. Forum* **2009**, *633–634*, 569–575. [CrossRef]
21. Mukhtarov, S.K.; Ermachenko, A.G. Influence of severe plastic deformation and heat treatment on microstructure and mechanical properties of a nickel-iron based superalloy. *Rev. Adv. Mater. Sci.* **2012**, *31*, 151–156.
22. Geng, P.; Li, W.; Zhang, X.; Deng, Y.; Kou, H.; Ma, J.; Shao, J.; Chen, L.; Wu, X. A theoretical model for yield strength anomaly of Ni-base superalloys at elevated temperature. *J. Alloys Compd.* **2017**, *706*, 340–343. [CrossRef]
23. Zheng, L.; Schmitz, G.; Meng, Y.; Chellali, R.; Schlesiger, R. Mechanism of intermediate temperature embrittlement of Ni and Ni-based superalloys. *Crit. Rev. Solid State Mater. Sci.* **2012**, *37*, 181–214. [CrossRef]
24. Rao, G.A.; Kumar, M.; Srinivas, M.; Sarma, D.S. Effect of standard heat treatment on the microstructure and mechanical properties of hot isostatically pressed superalloy Inconel 718. *Mater. Sci. Eng. A* **2003**, *355*, 114–125. [CrossRef]

25. Guedou, J.Y.; Lautridou, J.C.; Honnorat, Y. N18, PM superalloy for disks: Development and applications. *Superalloys* **1992**, *1992*, 267–276. [CrossRef]
26. Jia, C.L.; Ge, C.C.; Yan, Q.Z. Microstructure evolution and mechanical properties of disk superalloy under multiplex heat treatment. *Mater. Sci. Eng. A* **2016**, *659*, 287–294. [CrossRef]
27. Gayda, J. Dual Microstructure Heat Treatment of a Nickel-Base Disk Alloy. Technical Memorandum, NASA/TM—2001-211168 12 p. Available online: https://ntrs.nasa.gov/api/citations/20020013802/downloads/20020013802.pdf (accessed on 10 May 2023).
28. Mitchell, R.J.; Lemsky, J.A.; Ramanathan, R.; Li, H.Y.; Perkins, K.M.; Connor, L.D. Process development & microstructure & mechanical property evaluation of a dual microstructure heat treated advanced nickel disc alloy. *Superalloys* **2008**, *2008*, 347–356. [CrossRef]
29. Collins, D.M.; Stone, H.J. A modelling approach to yield strength optimization in a nickel-base superalloy. *Int. J. Plast.* **2014**, *54*, 96–112. [CrossRef]
30. Ning, Y.; Yao, Z.; Guo, H.; Fu, M.W. Structural-gradient-materials produced by gradient temperature heat treatment for dual-property turbine disc. *J. Alloys Compd.* **2013**, *557*, 27–33. [CrossRef]
31. Gayda, J.; Gabb, T.P.; Kantzos, P.T. The effect of dual microstructure heat treatment on an advanced nickel-base disk alloy. *Superalloys* **2004**, *2004*, 323–329. [CrossRef]
32. Jiang, R.; Everitt, S.; Lewandowski, M.; Gao, N.; Reed, P.A.S. Grain size effects in a Ni-based turbine disc alloy in the time and cycle dependent crack growth regimes. *Int. J. Fatigue* **2014**, *62*, 217–227. [CrossRef]
33. Zhang, W.; Huang, S.; Tian, Q.; Qing, H.; Xu, G.; Zhao, G.; Zhang, B. Microstructure control and mechanical properties of new developed C&W superalloy GH4175 at 800 °C. *IOP Conf. Ser. Mater. Sci. Eng.* **2018**, *452*, 022123. [CrossRef]
34. Jiang, R.; Wang, Y.C.; Zhang, L.C.; Chen, Y.; Zhang, H.; Wang, Z.B.; Song, Y.D. Fatigue crack propagation behavior of the grain size transition zone in a dual microstructure turbine disc. *Int. J. Fatigue* **2023**, *172*, 107647. [CrossRef]
35. Gabb, T.P.; Telesman, J.; Kantzos, P.T.; O'Connor, K. Characterization of the Temperature Capabilities of Advanced Disk Alloy ME3. Technical Memorandum, NASA/TM-2002-211796 51 p. Available online: https://ntrs.nasa.gov/api/citations/20020081280/downloads/20020081280.pdf (accessed on 10 May 2023).